J. Fluid Mech. (1984), *vol.* 138, *pp.* 185–196
Printed in Great Britain

A laboratory study of stratified accelerating shear flow over a rough boundary

By S. A. THORPE
Institute of Oceanographic Sciences, Wormley, Godalming, Surrey, U.K.

(Received 24 March 1983)

Experiments are made in which a stratified shear flow, accelerating from rest and containing a level where the direction of flow reverses, is generated over a rough floor. The roughness elements consist of parallel square bars set at regular intervals normal to the direction of flow. Radiating internal gravity waves are generated in the early stages of flow, whilst flow separation behind the bars produces turbulent mixing regions which eventually amalgamate and entirely cover the floor. This turbulent layer spreads vertically less rapidly than the internal waves. Observed features of the waves are compared with those predicted by a model in which the floor is assumed to be sinusoidal, and fair agreement is found for the amplitude, phase and vertical wavenumber of the waves, even when the latter becomes large.

The rate of spread of the turbulent layer depends on the separation of the bars. Some interaction between the turbulence and the internal waves occurs near the edge of the turbulent layer. Wave-breaking is prevalent and the vertical scale of the waves is affected by turbulent eddies. The radiating internal waves are suppressed by replacing the bars by an array of square cubes, but there is continued evidence of features resembling internal waves near the boundary of the turbulent region. Structures are observed which bear some similarities to those found at the foot of the near-surface mixing layer in a lake.

1. Introduction

The results of earlier experiments on shear flow of stratified fluid over a sinusoidal floor or past a small obstacle (Thorpe 1973, 1981, hereinafter referred to as I; Koop 1981), led us to ponder on the relevance of the study to naturally occurring flows over a rough topography, which would itself generate significant turbulence as well as internal waves. We have made some further experiments which are described below. In these the flow is transient, a feature of naturally occurring flows. The development of waves, eddies shed from roughness elements, and subsequently turbulence, can be followed from an initial state of rest. The experiments reveal processes occurring near the edge of the turbulent layer which have some resemblance to those observed near the foot of the near-surface mixing layer in a lake, but a quantitative comparison is not possible. The purpose of this note is to draw attention to some of the processes and complex interactions that may occur and to the need for further field observations, rather than to make any definite conclusions about which processes are dominant.

2. Experiments

The experiments were made in a tilting tube, the apparatus used in our previous experiments, and details of the methods employed are described in I. The present experiments were similar in most respects except for the replacement of the false sinusoidal floor by a flat aluminium plate to which were fixed certain 'roughness' elements. In the majority of experiments these were simply bars of 1.27 cm square section placed at regular intervals at right-angles to the tube length and extending across its 10 cm width except for 4.8 mm gaps at each end, which allowed the stratified brine solution to flow along the floor of the tube during filling. In spite of these gaps, the presence of the bars caused some mixing, and the density gradient was not uniform below the level of the top of the bars. The plate reduced the effective depth of the tube to 15.8 cm.

The square ends of the bars can be seen in figure 1. This shows shadowgraphs of the early stages of flow at equal time intervals after the tube, filled with brine of uniform density gradient, was tilted from the horizontal through an angle $\alpha = 7.6°$ down on the right as shown in the figure. (This tilt is the same in other figures, but has been removed in the reproductions.) The basic flow is a uniformly accelerating shear flow, fluid moving to the right in the lower part of the tube and to the left in the upper part. The shadowgraph pattern is repeated between successive bars, and this repetition in the general pattern continues at later times. Fine-scale structures, symptomatic of turbulent mixing, develop near the grid bars. In the later stages (*f*, *g*) tilted bands are seen above the turbulent region; these are due to internal gravity waves.

Figure 2 shows mosaics, (*a*, *b*), formed by a series of photographs at equal time intervals of the same section between two neighbouring bars in two experiments with the same angles of tube tilt $\alpha = 7.6°$, and similar initial density gradients with stability frequency N. The figure shows, with time increasing from left to right, the development of the turbulent layer and the internal waves. Part (*a*) shows shadowgraph images. The serrated edge of the upper boundary is an artifact due to a slight camera misalignment. Part (*b*) shows layers of dark dye in experiments with the same separation $d = 11.43$ cm between the centres of neighbouring bars, whilst (*c*) is a computer simulation which we describe in §3. The last photograph in each of the mosaics extends beyond the section shown in the others and indicates the degree of uniformity in the flow pattern at this stage of development. The bottom roughness here appears to be the k-type (Perry, Schofield & Joubert 1969), the height of the bars playing a role in determining the eddy scale of the turbulence. The upwards propagation of the internal waves can be seen, with evidence of overturning, development of static instability, in the dark dye layers ahead of the turbulent layer. The waves appear similar to those reported in I, with waves breaking as they approach their critical levels below mid-depth in the accelerating flow. They appear to be little affected by turbulence except close to its leading edge. The dye layers fail entirely to portray the high mode structure of the internal wave field, which, by the end of the sequence, extends close to the level near mid-tube depth where the flow reverses direction. In other experiments with different d, the vertical wavenumber at a given time after tilt was found to increase as d decreased.

Turbulence causes the dye in the lower layers to diffuse and the layers to amalgamate. The edge of the turbulent layer seen in figure 2 (*a*) is quite sharp and there are regions of large curvature in density, the dark shadows in (*a*), close to this edge, consistent with the wave overturning, or breaking, seen in the dye layers. A vertical

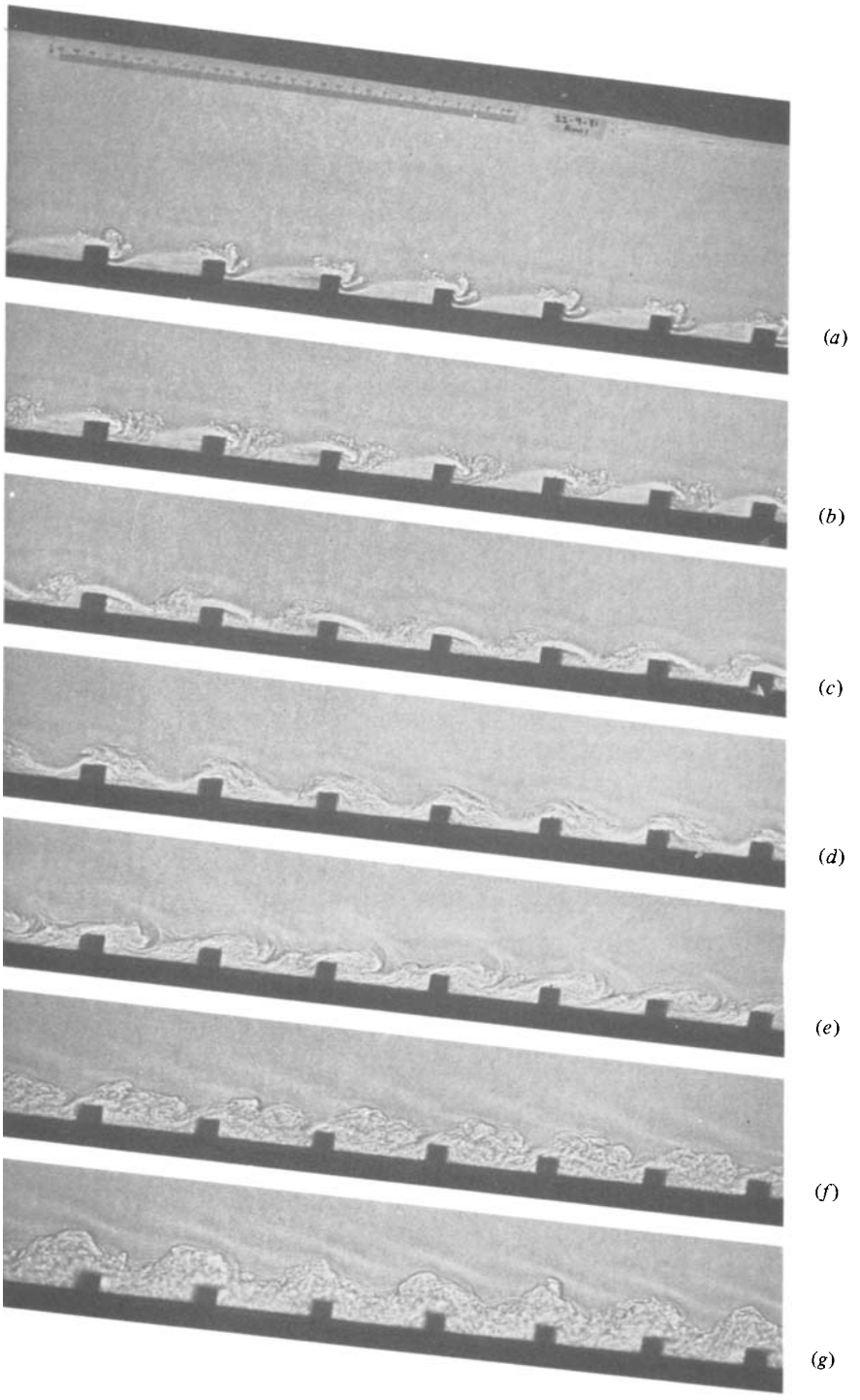

FIGURE 1. Shadowgraph images of accelerating flow over horizontal bars with $d = 7.62$ cm, $N = 2.45$ rad s^{-1}; (*a*) 0.48 s after tube was tilted; (*b*)–(*g*) at 0.52 s intervals.

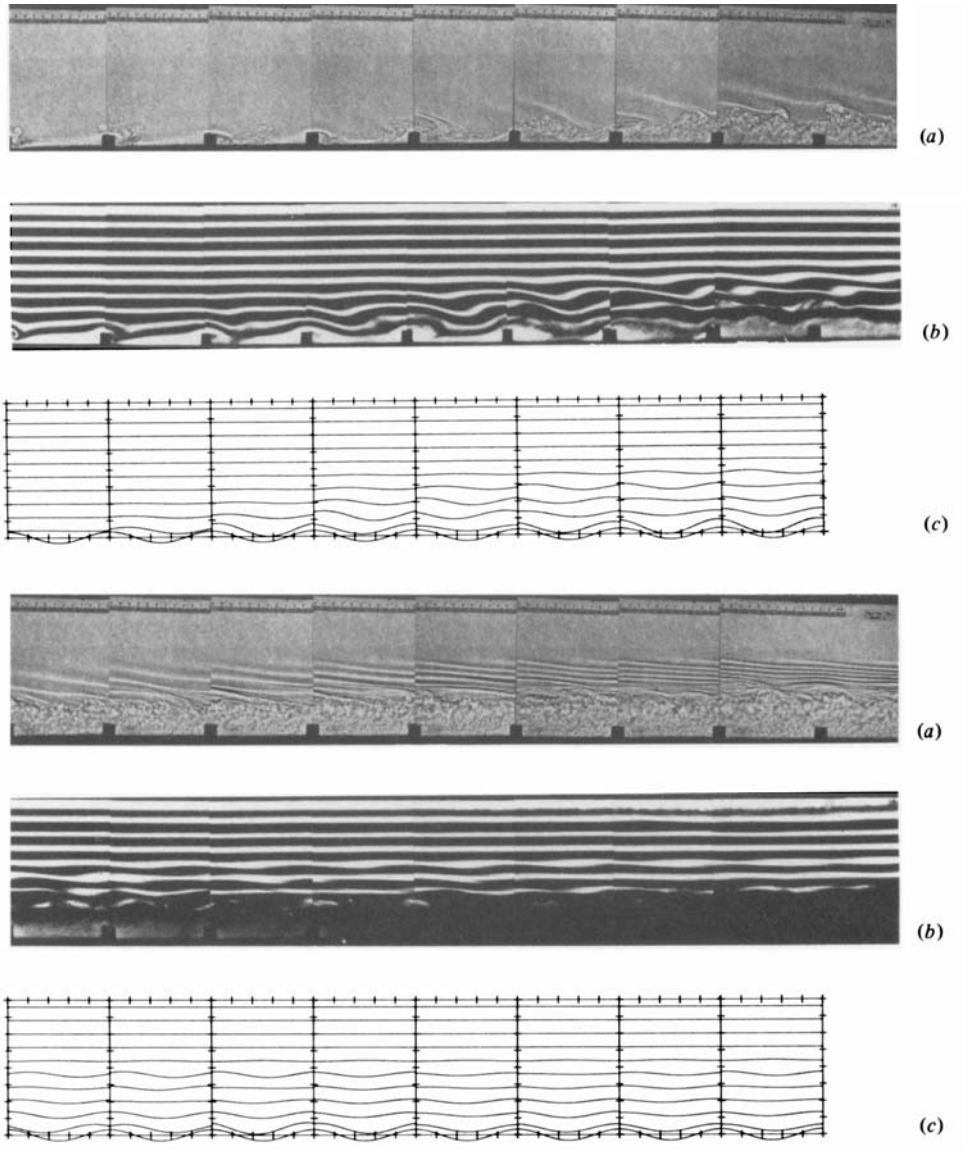

FIGURE 2. (*a*) Shadowgraph images, (*b*) dye layers, and (*c*) computed isopycnal surfaces at intervals of (*a*) 0.53 s (starting at 0.51 s and ending 8.43 s after tilt) and (*b*), (*c*) 0.53 s (starting at 0.22 s after tilt), time increasing to the right, with $d = 11.43$ cm, $N = 2.55$ rad s^{-1}. The Richardson number of the flow above the turbulent layer decreases as t^{-2} during the experiment to about 0.12 at the end.

profile of density using a single-electrode conductivity probe is shown in figure 3. This clearly demonstrates the appreciable changes to the density structure caused by the internal waves, the development of a knee in the profile near the top of the turbulent layer and the relatively uniform density structure in the turbulent layer itself.

The variation of the depth of the turbulent layer with time is shown in figure 4 for three experiments with similar values of N but different values of d. For the smallest value, $d = 3.81$ cm, the shadowgraphs of the early stages of the accelerating flow showed that vortices formed, filling the regions between neighbouring bars. The

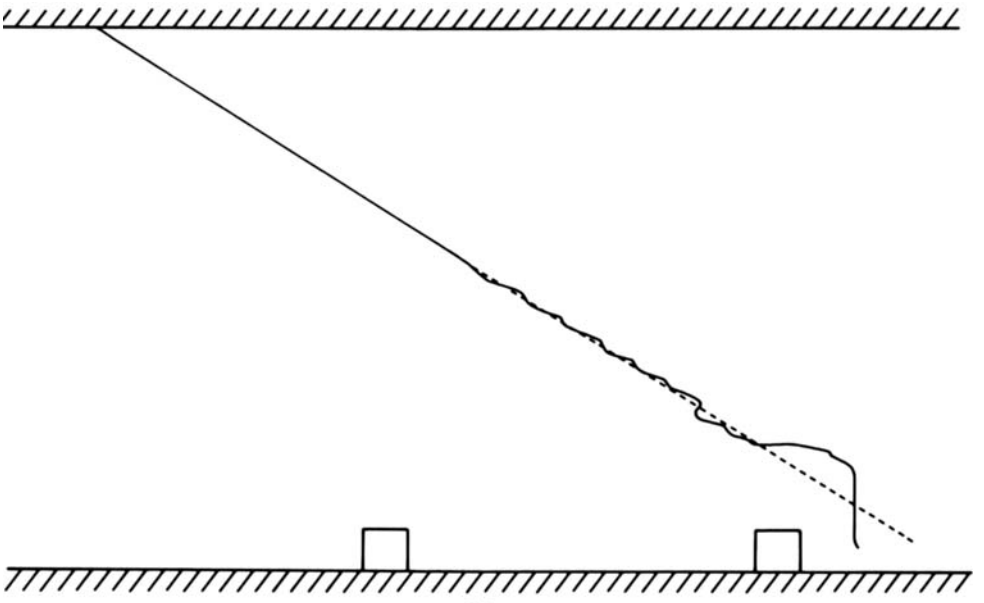

(*a*)

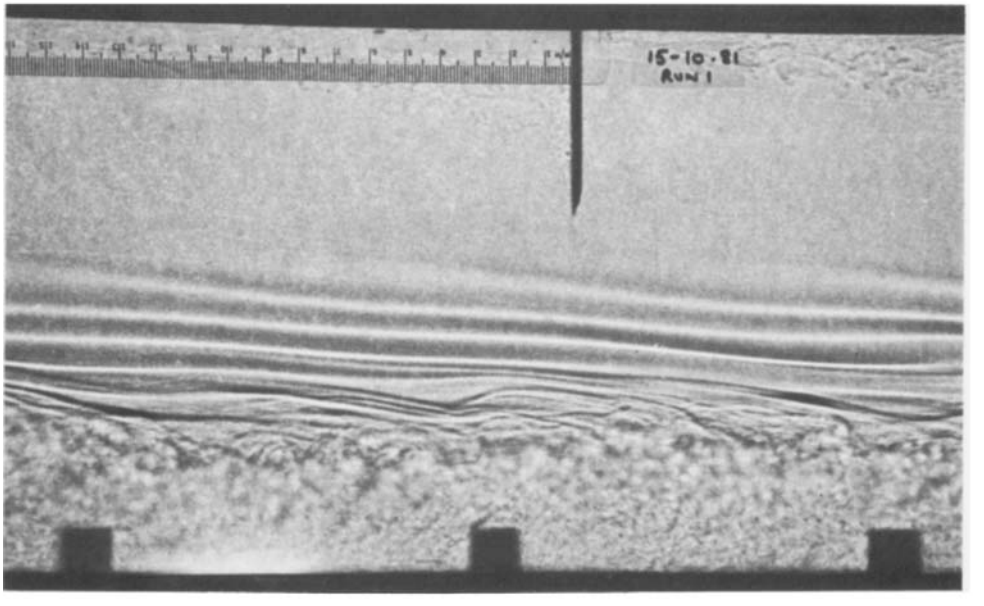

(*b*)

FIGURE 3. (*a*) Conductivity profile through waves and turbulent layer; $N = 2.50\ \mathrm{s}^{-1}$, $d = 11.43$ cm, $\alpha = 7.6°$. The dashed line shows the profile made before the tube was tilted. The full line is the profile begun 6.32 s after the tilt. The probe was lowered with mean speed 10.8 cm s^{-1}, and is shown in descent in the shadowgraph image in (*b*).

roughness was thus of the *d*-type, and the full vertical scale of the bars was not effective in disturbing the overlying flow. For $Nt > 8$ the turbulent layer was less extensive than for the *k*-type wall roughness of the other two experiments.

Attempts were made to produce a floor of more uniform roughness so as to reduce the generation and effect of the internal waves. A regular diamond array of cubes

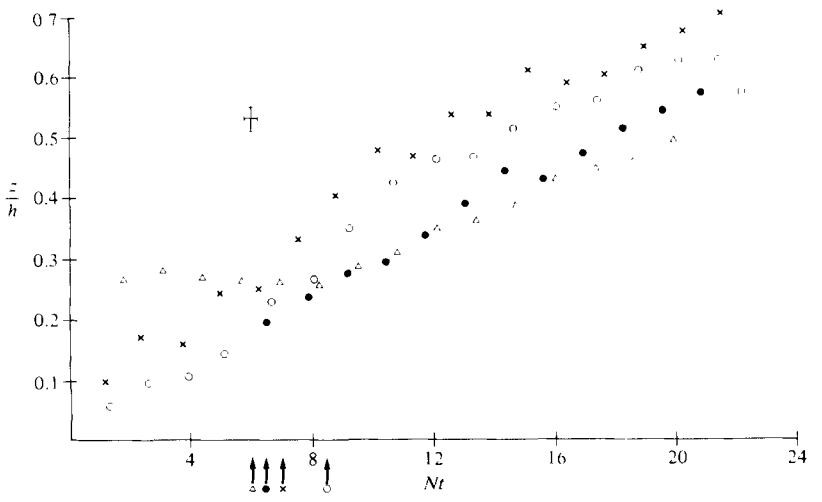

FIGURE 4. The mean height z of the turbulent layer, plotted as a fraction of the half-depth h of the tube, versus Nt, where t is the time after the tube was tilted. The points correspond to: △, $d = 3.81$ cm, $N = 2.49$ rad s^{-1}; ×, 7.62 cm, 3.45 rad s^{-1} (partly shown in figure 1); ○, 11.45 cm, 2.55 rad s^{-1} (figure 2a); ●, diamond array, 2.44 rad s^{-1} (figure 5). The estimates of z/h include the volume of the roughness elements and should be reduced by 0.054, 0.027, 0.018 and 0.021 respectively in the four cases if they are to represent only the turbulent volume. The arrows on the Nt-axis indicate the times at which the turbulent layer became continuous along the floor of the tube. The equivalent Richardson number of the mean flow is $(Nt\sin\alpha)^{-2}$.

was constructed. This consisted of rows of 1.27 cm cubes, each with centre 3.81 cm from its neighbour, placed across the tank, the cubes in adjacent rows being staggered so as to be halfway between those in the next row, and the centre of each row being 1.84 cm from its neighbour. This pattern should produce a near-optimum roughness length (see Raupach, Thom & Edwards 1980, figure 1). The cube pattern is similar to that shown in their figure 3F). Figure 5 shows a shadowgraph image of the turbulent layer produced over this rough boundary. Tilted structures resembling internal waves are still visible at the leading edge of the layer, and are apparently generated locally by turbulent eddies, but they no longer have the regularity of those in the earlier experiments and do not propagate far beyond the turbulent layer. They are, however, coherent over scales much exceeding those of the roughness elements, apparently also exceeding those of the turbulent eddies. The growing thickness of the turbulent layer is shown in figure 4.

3. Discussion

In I we describe a two-dimensional numerical model of internal waves produced by an inviscid accelerating flow over a sinusoidal floor. It is assumed that the density gradient is initially uniform and that the flow starts from rest. We have used the linearized form of the model to produce the first-order wave patterns shown in figure 2(c). We have similarly constructed vertical profiles of the modulus of the first-order density perturbation at intervals of 0.2 s (figure 6) for comparison with the shadowgraph images (a) in figure 2. The height of the bars was used as the height of the sinusoidal waves at the floor in the numerical model, and we employed a grid with 400 points in the vertical to properly resolve the vertical wavelength.

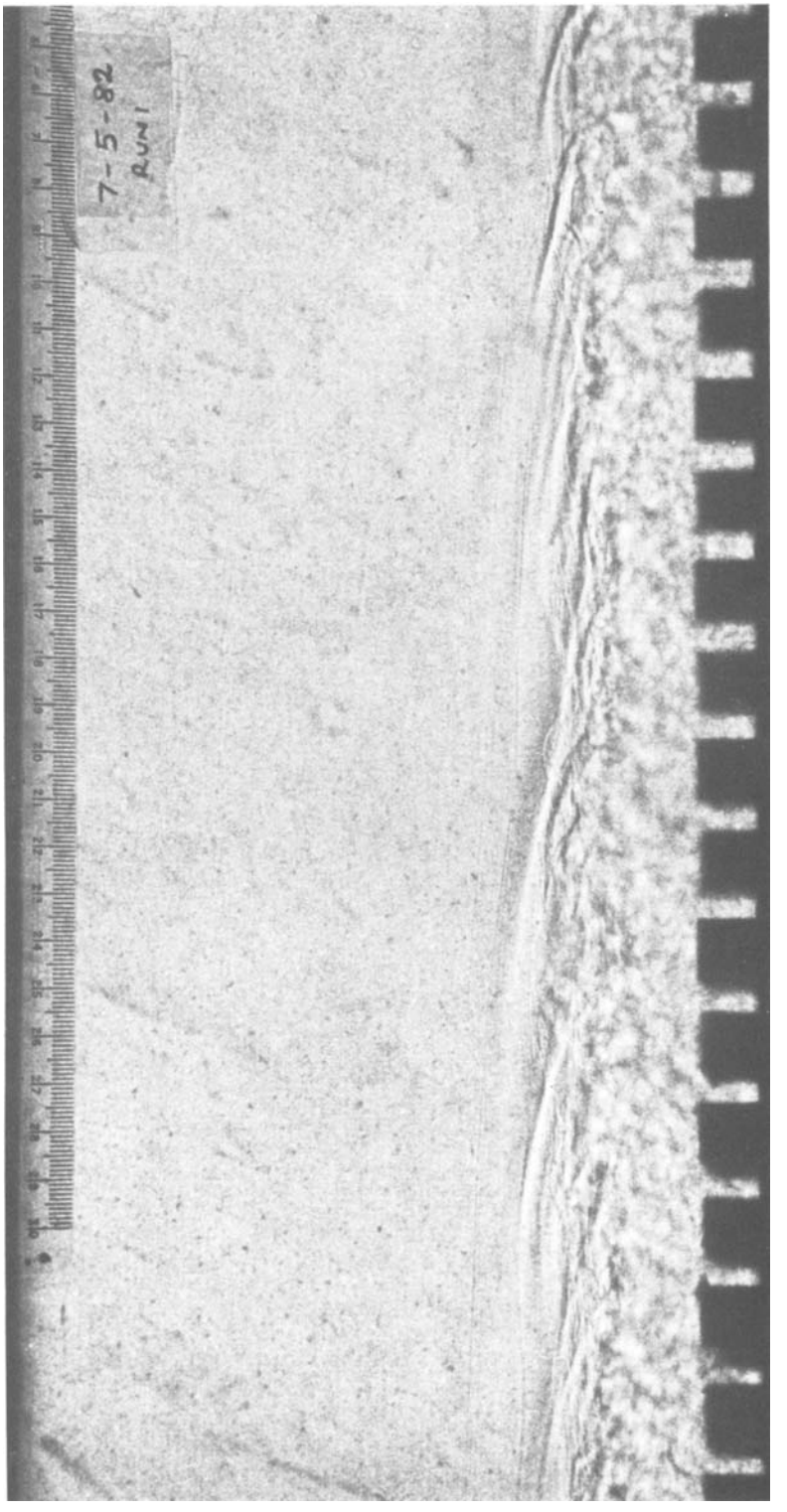

FIGURE 5. Shadowgraph of flow over a diamond array of cubes (see text) taken 7.5 s after the tube was tilted; $N = 2.46$ rad s^{-1}, $\alpha = 7.6°$.

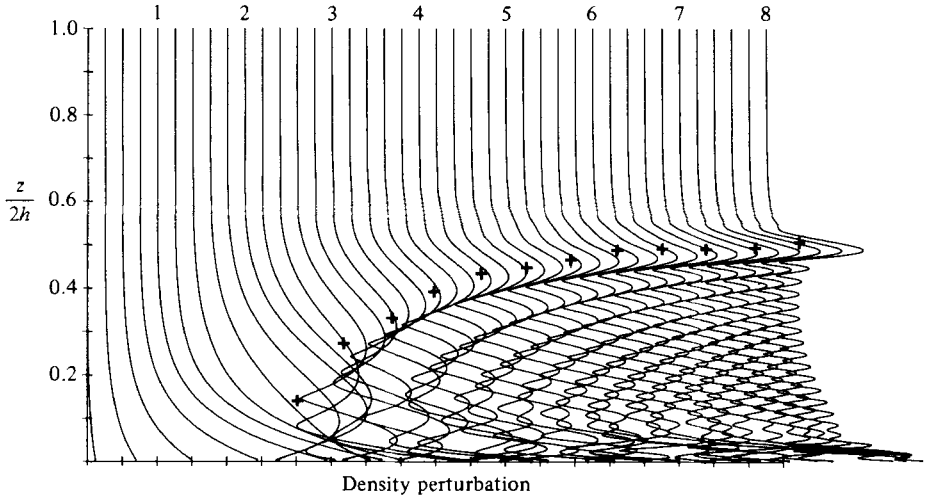

FIGURE 6. Vertical profiles of density perturbations due to internal waves drawn at intervals of 0.2 s and calculated for conditions corresponding to those in figure 2(*a*). Each successive profile has been displaced to the right by an amount corresponding to the separation of the profiles at the top, $z/2h = 1.0$, where z is the distance from the floor of the tube. The times in seconds are marked at the top. The crosses mark the greatest height at which internal waves can be seen in figure 2(*a*).

The comparison of predicted and observed wave amplitude and phase (e.g. as shown in figures 2*b*, *c*) was generally as favourable as could be expected, considering that the model has a sinusoidal corrugation, not bars, and recalling the importance of the nonlinear effects discussed in I and the effect of flow separation, especially when $d = 3.81$ cm, in reducing the effective roughness of the bottom. It may be noticed that in neither the experiments nor the computer simulations do the waves reach the mid-depth level with as large an amplitude as found in I, where larger wavelengths were considered. This is probably because of the effect, illustrated in figure 2 of I, that, the shorter the horizontal wavelength, the less distance do wave rays propagate vertically in the accelerating flow.

It would have been more appropriate to have compared the second derivative of the density perturbation with the intensity of light in the shadowgraphs, but the density perturbation itself (e.g. figure 6) serves well enough to indicate the propagation of the waves seen in the shadowgraph images and the variation in their vertical wavenumber. Again the comparison of observations and the model was fairly good, although an almost constant time discrepancy of 0.35–0.65 s was apparent in detailed comparison of the vertical wavenumber of the waves, the observed lagging the predicted. Since, however, time in the experiments is measured from midway between the time at which tilt is begun and the time at which it is completed (the interval being typically 0.3–0.5 s), whereas in the model the tilt is effectively instantaneous, the flow accelerating from rest in an initially tilted tube, this discrepancy is perhaps not significant. The predicted vertical spread of the waves is in fair agreement with observations, and the numerical model appears capable of dealing with waves of high wavenumbers. The observed waves remain below the position of the critical level where the flow reverses.

The vertically propagating waves produced by flow over the fixed corrugations in the floor are generated predominantly during the early stages of flow (see I, §1), that

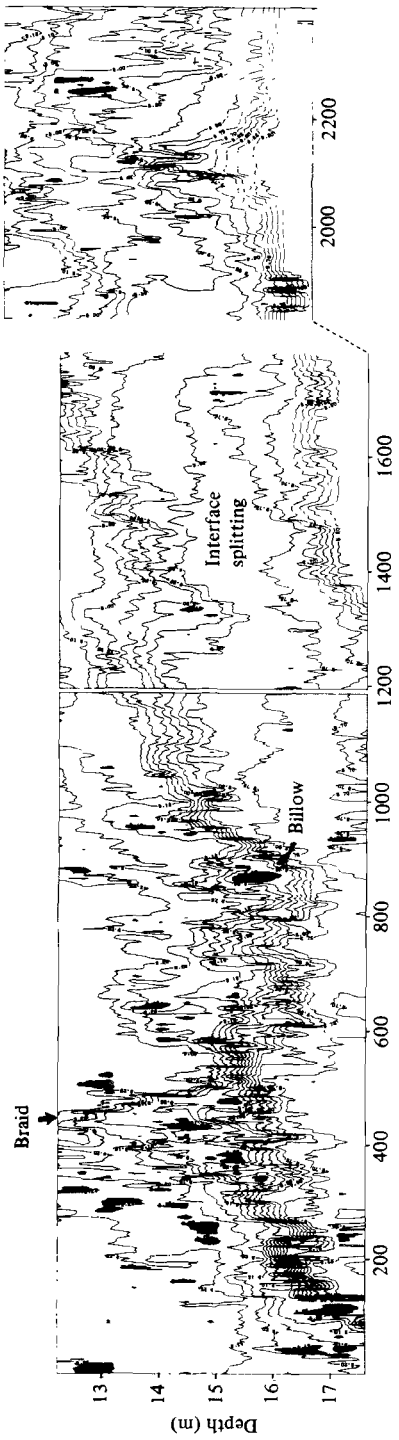

FIGURE 7. Temperature contours, depth *vs.* time, from a vertical array of 13 equally spaced thermistors moored in Loch Ness (for a fuller description see Thorpe 1978). Temperatures are averages over 5 s. The array spans the base of the near-surface mixing layer. Contours are at 50 mC intervals. There is a short break in the record near 1200 s, and the array was raised by 1 m after 1800 s. The wind speed was about 10.5 m s^{-1}. The region of large temperature gradient seen near 16.4 m depth at 200 s was the base of the near-surface mixing layer (determined by vertical profiles). The velocity difference across this large-gradient region was about 6.5 cm s^{-1}, making the gradient Richardson number there approximately 0.35.

is when the flow U at the boundary, ignoring the effects of the roughness elements, is less than $Nd/2\pi$. In the absence of viscosity or floor roughness,

$$u(z) = N^2 zt \sin\alpha, \tag{1}$$

where z is measured from mid-depth, and so $U = N^2 ht \sin\alpha$, where h is half the depth of the tube, and free waves are emitted only for times less than $d/2\pi Nh \sin\alpha$, typically 0.24 s for the experiments with $d = 3.81$ cm, or 0.68 s for those with $d = 11.43$ cm. These times are short compared with those required to develop the turbulence. It can therefore be anticipated that, provided the waves propagate vertically so rapidly as to remain above the turbulent layer, they will be little modified by it. Trapped waves in the region close to the rough boundary will be more severely affected. The vertically propagating waves formed in the early stages of flow subsequently have horizontal speeds through the flow which are very much less than that of the local flow itself. Consequently the waves are primarily advected, and large vertical wavenumbers develop as the result of the tilting of waves over their neighbours in the shear flow. One effect of the shear is thus to produce structures which intersect the isopycnal surfaces at decreasingly small angles and which are coherent over scales greatly exceeding that of the forcing scale d. Similar effects can be seen in experiments in which a pre-existing train of internal waves is distorted by the acceleration in the mean flow (Thorpe 1978*a*, see especially figure 8). A note about the expected nature of the disturbances at large times is included in the Appendix.

There is evidence (see figure 5) that the turbulent eddies themselves force internal waves (see e.g. Piat & Hopfinger 1981), though this cannot be quantified in the present experiments. Signs of interaction between the turbulent layer and the internal waves are only evident near the edge of the turbulent layer, where turbulent eddies are seen to rise, enhance the density curvature, and locally reduce the vertical wavelength of the waves, and where the density gradients are largest, and some wave-breaking occurs. This contrasts with the experiments in I, in which wave-breaking was most severe in the vicinity of the critical level at tube mid-depth where the flow reverses, rather than below.

Some measurements of velocity were attempted by following individual features in the shadowgraph or dye, but apart from revealing a flow less than that predicted by the inviscid laminar-flow model (1) in the turbulent region but comparable to (1) in the region above, the results were not sufficiently precise for us to draw any detailed conclusions.

Some comparisons with natural flows are instructive, although detailed observations in the sea or lakes are few and generally insufficient. The steplike structure in the density profile (see figure 3) is similar to that often found in and below the ocean thermocline (Woods 1968). Further studies of transience in density structures occurring in the upper thermocline of the ocean would be useful. Fine-scale measurements of the temperature field at the foot of the near-surface turbulent mixing layer of Loch Ness, illustrated in figure 7, show a variety of structures, notably the narrow tilted thermal fronts or 'braids' already seen in the mixing layer itself (Thorpe 1978*b*; Thorpe & Hall 1980, 1982) but not previously reported at the foot of the layer, and Kelvin–Helmholtz 'billows' (Thorpe *et al.* 1977). There is also evidence that the layer of large density gradient at the top of the seasonal thermocline occasionally splits as shown in the figure, forming temporarily an almost uniform region between two tilted layers of high gradient. The horizontal extent of this region, estimated on the assumption that it is advected by the horizontal current, is about 35 m, greater than the mixing-layer thickness. This feature resembles wave overturn

seen near a critical level (see I, figure 5) or in the development of Kelvin–Helmholtz instability (Peltier, Hallé & Clark 1978), or the successive layers of high gradient found in the present experiment at the edge of the turbulent region (for example in figure 5). Further evidence of 'layer splitting' can be found in the vertical profiles of temperature measured during a storm at sea by Dillon & Caldwell (1978, see especially figures 1 and 3). These features appear to play a role in the entrainment of denser water into the mixing layer, and deserve more attention. Information is also needed about the velocities and integral scales of the turbulence in the near-surface mixing layer so that estimates can be made (Townsend 1968) of the internal waves it produces.

I am grateful to Alan Hall for his help in making the laboratory experiments and in obtaining the data for figure 5.

Appendix. Algebraic disturbances

A referee suggested that the algebraic disturbances discussed by Brown & Stewartson (1980) are precisely the kind of internal gravity waves observed in these experiments. Whilst this appears to be substantially correct, the effect of accelerating mean flow may be important in determining the mode of decay of the disturbances.

The linearized vorticity equation is, using (1),

$$\left(\frac{\partial}{\partial t}+\beta z t\frac{\partial}{\partial x}\right)\nabla^2\psi = g\left(\cos\alpha\frac{\partial}{\partial x}-\sin\alpha\frac{\partial}{\partial z}\right)\rho, \tag{A 1}$$

where ψ is the stream function, ρ is the density perturbation divided by a reference density, and $\beta = N^2\sin\alpha$.

Conservation of density gives

$$\left(\frac{\partial}{\partial t}+\beta z t\frac{\partial}{\partial x}\right)\rho = -\frac{N^2}{g}\frac{\partial\psi}{\partial x}. \tag{A 2}$$

Writing $t = \beta^{-\frac{1}{2}}\tau$ and $\rho = Nr(g\sin^{\frac{1}{2}}\alpha)^{-1}$, we have

$$\left(\frac{\partial}{\partial\tau}+z\tau\frac{\partial}{\partial x}\right)\nabla^2\psi = \left(\cot\alpha\frac{\partial}{\partial x}-\frac{\partial}{\partial z}\right)r, \tag{A 3}$$

$$\left(\frac{\partial}{\partial\tau}+z\tau\frac{\partial}{\partial x}\right)r = -\frac{\partial\psi}{\partial x}. \tag{A 4}$$

The term in $\partial r/\partial z$ did not appear in the equivalent equations considered by Brown & Stewartson, nor did the coefficient τ or $\cot\alpha$. If at $t = 0, \psi(x,z,0) = \alpha_1(x)$ and $r(x,z,0) = \alpha_2'(x)$, a particular integral of (A 3) and (A 4) is

$$r(x,z,\tau) = f_1(\tau)\,\alpha_1'(x-\tfrac{1}{2}z\tau^2)+f_2(\tau)\,\alpha_2'(x-\tfrac{1}{2}z\tau^2),$$

$$\psi(x,z,\tau) = f_1'(\tau)\,\alpha_1(x-\tfrac{1}{2}z\tau^2)+f_2'(\tau)\,\alpha_2(x-\tfrac{1}{2}z\tau^2),$$

where f_1 and f_2 are solutions of the equation

$$(4+\tau^4)f''+4\tau^3f'-2f(2\cot\alpha+\tau^2) = 0, \tag{A 5}$$

satisfying $f_1(0) = 0, f_1'(0) = 1, f_2(0) = 1, f_2'(0) = 0$ (see also Thorpe 1978, equation (11) with $l = 0$).

The solutions of (A 5) are no longer the hypergeometric functions F (or τ times F)

which Brown & Stewartson obtained. At large τ however, $f \sim \tau^q$, where $q = -1$ or -2, indicating a decaying, algebraic behaviour. This thus follows the behaviour of Brown & Stewartson's solution at large time ($q = -\frac{3}{2} \pm \nu$, where $\nu^2 = \frac{1}{4} - J$ and J is the steady mean-flow Richardson number) in the limit $J \to 0$. An example of an experiment in which algebraically decaying waves should be found in an almost steady flow is described by Thorpe (1978*a*, see experiment B after 5.5 s).

REFERENCES

Brown, S. N. & Stewartson, K. 1980 On the algebraic decay of disturbances in a stratified linear shear flow. *J. Fluid Mech.* **100**, 811–816.

Dillon, T. M. & Caldwell, D. R. 1978 Catastrophic events in a surface mixed layer. *Nature* **276**, 601–602.

Koop, C. G. 1981 A preliminary investigation of the interaction of internal gravity waves with a steady shearing motion. *J. Fluid Mech.* **113**, 347–386.

Peltier, W. R., Hallé, J. & Clark, T. L. 1978 The evolution of finite amplitude Kelvin–Helmholtz billows. *Geophys. Astrophys. Fluid Dyn.* **10**, 53–87.

Perry, A. E., Schofield, W. H. & Joubert, P. N. 1969 Rough wall turbulent boundary layers. *J. Fluid Mech.* **37**, 383–413.

Piat, J.-F. & Hopfinger, E. J. 1981 A boundary layer topped by a density interface. *J. Fluid Mech.* **113**, 411–432.

Raupach, M. R., Thom, A. S. & Edwards, I. 1980 A wind-tunnel study of turbulent flow close to regularly arrayed rough surfaces. *Boundary-Layer Met.* **18**, 373–397.

Thorpe, S. A. 1973 Turbulence in stably stratified fluids. A review of laboratory experiments. *Boundary-Layer Met.* **5**, 95–119.

Thorpe, S. A. 1978*a* On internal gravity waves in an accelerating shear flow. *J. Fluid Mech.* **88**, 623–639.

Thorpe, S. A. 1978*b* The near-surface ocean mixing layer in stable heating conditions. *J. Geophys. Res.* **83**, 2875–2885.

Thorpe, S. A. 1981 An experimental study of critical layers. *J. Fluid Mech.* **103**, 321–344.

Thorpe, S. A. & Hall, A. J. 1980 The mixing layer of Loch Ness. *J. Fluid Mech.* **101**, 687–703.

Thorpe, S. A. & Hall, A. J. 1982 Observations of the thermal structure of Langmuir circulation. *J. Fluid Mech.* **114**, 237–250.

Thorpe, S. A., Hall, A. J., Taylor, C. & Allen, J. 1977 Billows in Loch Ness. *Deep-Sea Res.* **24**, 371–379.

Townsend, A. A. 1968 Excitation of internal waves in a stably stratified atmosphere with considerable wind-shear. *J. Fluid Mech.* **32**, 145–171.

Woods, J. D. 1968 Wave-induced shear instability in the summer thermocline. *J. Fluid Mech.* **32**, 791–800.